

Optically engineering the topological properties of a spin Hall insulator

Balázs Dóra,^{1,*} Jérôme Cayssol,^{2,3,4} Ferenc Simon,¹ and Roderich Moessner³

¹*Department of Physics, Budapest University of Technology and Economics, Budafoki út 8, 1111 Budapest, Hungary*

²*LOMA (UMR-5798), CNRS and University Bordeaux 1, F-33045 Talence, France*

³*Max-Planck-Institut für Physik komplexer Systeme, Nöthnitzer Str. 38, 01187 Dresden, Germany*

⁴*Department of Physics, University of California, Berkeley, California 94720, USA*

(Dated: November 9, 2018)

Time-periodic perturbations can be used to engineer topological properties of matter by altering the Floquet band structure. This is demonstrated for the helical edge state of a spin Hall insulator in the presence of monochromatic circularly polarized light. The inherent spin structure of the edge state is influenced by the Zeeman coupling and not by the orbital effect. The photocurrent (and the magnetization along the edge) develops a finite, helicity dependent expectation value and turns from dissipationless to dissipative with increasing radiation frequency, signalling a change in the topological properties. The connection with Thouless' charge pumping and non-equilibrium Zitterbewegung is discussed, together with possible experiments.

PACS numbers: 03.65.Vf,72.40.+w,81.05.ue

Introduction. Topological insulators (TIs) are a focus of attention, not least due to their possible application in spintronics and quantum computation. They represent distinct states of matter with robust, topologically protected conducting helical edge/surface states [1, 2]. The importance of the spin-orbit interaction is reflected in their charge carriers having their spin locked to their momentum. In particular the two dimensional TI, namely the quantum spin Hall (QSH) state, has been predicted for a variety of systems including graphene [3], HgTe/CdTe [4] and InAs/GaSb [5] quantum wells, lattice models [6–8] and multi-component ultracold fermions in optical lattices [9–11]. Nevertheless, in all of these, the gapless helical edge state originates from a subtle band inversion [1, 2] which requires careful Bloch band structure engineering [3–11] as well as a high degree of sample control [12–14].

Bloch states and energy bands arise from spatially periodic Hamiltonians in condensed matter systems. Extending the periodicity in the time domain through a time-periodic perturbation increases tunability of the Hamiltonian: the temporal analogue of Bloch states (the Floquet states) can be manipulated via the periodicity and amplitude of the external perturbation.

Recently, topological phases of periodically driven quantum systems have been characterized [15] using Floquet theory, extending the time-independent topological classification [16–18]. Interestingly, novel topological edge states can be induced by shining electromagnetic radiation on a topologically trivial insulator, e.g. a non inverted HgTe/CdTe quantum well with no edge state in the static limit [19]. Besides, a time-dependent perturbation may also be harmful for the coherence of the edge/surface states of TIs by introducing dissipation. It is therefore natural to investigate to what extent the steady state of a TI remains robust against time-dependent perturbations and how the electrical and mag-

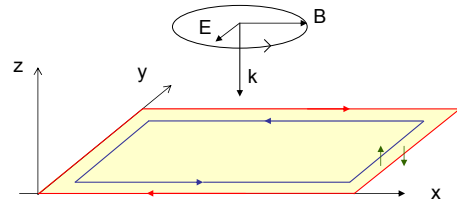


FIG. 1. (Color online) The quantum spin-Hall insulator (light yellow rectangle) with its helical edge state (counterpropagating red/blue arrows) in a circularly polarized electromagnetic field with frequency ω and wave vector k . In the plane $z = 0$ the rotating magnetic field $\mathbf{B}(t) = B_0(\cos \omega t, \sin \omega t)$ is perpendicular to the σ^z direction (vertical green arrows). A small tilting from the z axis does not influence our results.

netic properties are altered.

In this work, we consider the one-dimensional helical edge state of a QSH insulator in a circularly polarized radiation field. When increasing the radiation frequency, the steady edge state is found to switch from a dissipationless charge pumping to a dissipative transport regime. We characterize those regimes by their dc and ac photocurrent responses and provide experimental proposals to measure them. Finally, we demonstrate that the photocurrent, the magnetization and the Zitterbewegung phenomenon are ruled by the very same unit vector, whose winding number determines a topological invariant for the system. Although, our predictions could be tested by experiments similar to those in graphene [20] and HgTe/CdTe quantum wells [21], they rely on a different coupling mechanism, that is Zeeman coupling rather than orbital coupling.

Model. We consider a QSH insulator located in the xy plane and radiated by a circularly polarized electromagnetic field $\mathbf{A}(t) = A_0(\cos(\omega t - kz), \sin(\omega t - kz))$ with wave-vector k and frequency ω , whose sign determines the helicity of the polarization (Fig. 1). The time-

dependent Hamiltonian of the QSH edge reads [22]

$$H(t) = v_F \sigma^z (p - eA_x(t)) + g [\sigma^+ e^{-i\omega t} + h.c.], \quad (1)$$

where σ is the vector of Pauli matrices representing the physical spin of the electron, p the momentum along the one-dimensional channel, v_F the Fermi velocity, and e the electron charge. The electric current operator [23] is $j = ev_F \sigma^z$. The circularly polarized radiation acts on both the orbital motion through the vector potential $A_x(t) = A_0 \cos \omega t$ and on the electron spin through the Zeeman coupling $g = g_{\text{eff}} \mu_B B_0$, g_{eff} being the effective g -factor and μ_B the Bohr magneton. Nevertheless at high frequency, the orbital effect can be safely neglected according to a simple semi-classical argument (for a more rigorous treatment, see [23]). An electron travelling at the speed v_F in an electric field $E_0 = A_0 \omega = cB_0$ (c the speed of light) during a time $1/\omega$ picks up an energy $v_F e E_0 / \omega$ from the vector potential which has to be compared to the smallest energy quantum it can absorb, $\hbar \omega$ (restoring original units). Hence in the regime $v_F e E_0 / \omega \ll \hbar \omega$, only the time-dependent Zeeman effect is effective, and in this respect, our effective Hamiltonian differs significantly from other studies on similar systems [24–31] with dominant orbital effect. For typical parameters ($v_F = 10^5$ m/s, laser power of 1 mW focused onto an area of 1 mm², yielding $E_0 \approx 600$ V/m), this requires $\omega \gg 0.5$ THz, i.e. lasers operating in the far infrared or in the visible range. We also assume that $\hbar \omega$ is smaller than the bulk gap of the 2D insulator.

Floquet states.— In order to study the steady state of the edge, we solve the time-dependent Schrödinger equation, $i\partial_t \Psi_p(t) = H(t) \Psi_p(t)$, with $A_x = 0$ in Eq. (1). Applying Floquet theory [32, 33], the solution of the time-dependent Schrödinger equation is written as

$$\Psi_p(t) = \exp(-iE_\alpha(p)t) \Phi_\alpha(p, t), \quad (2)$$

where $E_\alpha(p)$ is the Floquet quasienergy, and $\Phi_\alpha(p, t) = \Phi_\alpha(p, t + T)$ with $T = 2\pi/\omega$. From this, physically equivalent steady states can be created [32] by shifting the quasienergy $E_{n,\alpha}(p) = E_\alpha(p) + n\omega$ and defining $\Phi_{n,\alpha}(p, t) = \Phi_\alpha(p, t) \exp(in\omega t)$ where n is a relative integer. Then, the quasienergy and wavefunction are obtained as

$$E_\alpha(p) = \frac{\omega}{2} + \alpha\lambda, \quad (3)$$

$$\Phi_\alpha(p, t) = \frac{1}{\sqrt{2\lambda}} \begin{pmatrix} \sqrt{\lambda + \alpha(v_F p - \omega/2)} \\ \alpha \exp(i\omega t) \sqrt{\lambda - \alpha(v_F p - \omega/2)} \end{pmatrix}, \quad (4)$$

where $\alpha = \pm 1$, $\lambda = \sqrt{g^2 + (v_F p - \omega/2)^2}$. The quasienergies describe the opening of a gap of size g around $\omega/2$ [23]. This photoinduced gap is located at momentum $p = \omega/2v_F$ and stems from one-photon assisted processes. A given $\Psi_\alpha(p, t)$ describes the steady state where an initial state with $g = 0$ would evolve adiabatically if we switch on the magnetic field at $t = -\infty$.

We introduce the average energy [33], which is used to identify the filled Floquet states [27], in analogy to the stationary situation [23], as

$$\bar{E}_\alpha(p) = \Psi_p^\dagger(t) H \Psi_p(t) = \alpha \left[\lambda + \frac{\omega(v_F p - \omega/2)}{2\lambda} \right], \quad (5)$$

which is always single valued as opposed to the ladder of quasienergies $E_{n,\alpha}(p)$.

High and low frequency regimes.— It is natural to distinguish high and low frequencies in terms of the ratio of the Zeeman coupling strength g and radiation frequency ω . More specifically the Floquet spectrum happens to be gapped for $|\omega| < 4g$ and gapless for $|\omega| > 4g$. In the low frequency regime, the bands are well separated by the photoinduced gap for any momentum, the ($\alpha = -1$)-band being the fully occupied one. In contrast, in the high frequency regime ($|\omega| > 4g$), the states of the ($\alpha = +1$)-band become lower in energy than the ones of the ($\alpha = -1$)-band within the momenta range $\omega_- < v_F p < \omega_+$ with $4\omega_\pm = \omega \pm \sqrt{\omega^2 - 16g^2}$ [23]. The band touching at $|\omega| = 4g$ has a clear signature in the total energy which picks up a singular contribution as

$$E_{\text{tot}} = E_s(g, \omega) + \frac{\rho_0 \sqrt{g}}{3} (|\omega| - 4g)^{3/2} \quad (6)$$

for $|\omega| \gtrsim 4g$, while $E_s(g, \omega) = \rho_0 [\omega^2/4 - g^2 \ln(2W\sqrt{e}/g)]$ is a *smooth* function of $(\omega - 4g)$. The lattice constant is denoted by a , $\rho_0 = a/\pi v_F$, and W is a high energy cut-off. The exponent 3/2 appears also in the orbital contribution to the ground state energy of two dimensional Dirac fermions [34].

Electromagnetic response and topological invariants.— The electromagnetic response of the QSH edge state is more easily detected than the singularity in the ground state energy Eq. (6). As a main signature, a dc photocurrent $\langle j \rangle$ is generated along the edge whose direction is determined by the helicity of the circular polarization. Interestingly there is no accompanying ac-current in the absence of orbital coupling. Moreover the current operator being $j = ev_F \sigma^z$, such a dc current also corresponds to a steady state magnetization $\langle \sigma^z \rangle$ along the edge.

We have obtained the full dependence of the dc photocurrent/steady state magnetization for any arbitrary frequency within the bulk gap of the QSH insulator. Besides we demonstrate that the dc photocurrent is directly related to a topological property of the time-dependent Floquet state, that is the topological invariant:

$$\mathcal{C}_\alpha = \frac{1}{2} \sum_p \int_0^T dt \hat{\mathbf{d}}_{\alpha,p}(t) \cdot \left(\partial_p \hat{\mathbf{d}}_{\alpha,p}(t) \times \partial_t \hat{\mathbf{d}}_{\alpha,p}(t) \right). \quad (7)$$

This Chern number \mathcal{C}_α , associated with the band α , is the winding number of the mapping, $(p, t) \rightarrow \hat{\mathbf{d}}_{\alpha,p}(t) =$

$\Phi_{\alpha}^{+}(p, t)\sigma\Phi_{\alpha}(p, t) = \alpha(g \cos \omega t, g \sin \omega t, v_F p - \omega/2)/\lambda$, between the 1+1 dimensional extended Brillouin zone in (p, t) space and the unit sphere [1, 19], the summation being taken over occupied bands.

In the low frequency regime ($|\omega| < 4g$), the dc photocurrent

$$\langle j \rangle = \int_{-\infty}^{\infty} \frac{e v_F dp}{2\pi} \hat{\mathbf{d}}_{-,p}^z(t) = \frac{e\omega}{2\pi}, \quad (8)$$

is independent of the coupling strength g , the charge pumped within one cycle (T) being exactly the unit charge. This adiabatic pumped current has been considered in Ref. [22]. As noticed by Thouless [35], the integer charge pumped across a 1D insulator in one period of an (adiabatic) cycle is a topological invariant that characterizes the cycle. Here this specific quantization of charge stems directly from the quantized Chern number

$$\mathcal{C}_{\alpha} = - \int_{-\infty}^{\infty} dp \frac{\alpha \text{sign}(\omega) v_F g^2}{2\lambda^3} = -\alpha \text{sign}(\omega), \quad (9)$$

the ground state being the filled $\alpha = -1$ band, yielding $\langle j \rangle = e\mathcal{C}_{-}/T$. The dc current is therefore dissipationless, protected by a photoinduced gap[23].

At high frequency, $|\omega| > 4g$, the system undergoes a photoinduced band inversion and the Chern number

$$\mathcal{C}_{\alpha} = -\alpha \text{sign}(\omega) \left(1 - \sum_{s=\pm 1} s \frac{\sqrt{2\omega\omega_s}}{\omega} \right) \quad (10)$$

is no longer quantized (Fig. 2), reminiscent of the transfer of Chern number between equilibrium bands which touch. We note that the Chern number is continuous at the transition $|\omega| = 4g$ and vanishes slowly as $\mathcal{C}_{\alpha} = -\alpha 2g/\omega$ for $|\omega| \gg g$.

The corresponding dc photocurrent is

$$\langle j \rangle = \frac{e}{2\pi} \left(\omega - \sum_{s=\pm 1} s \sqrt{2\omega\omega_s} \right). \quad (11)$$

While the current still satisfies $\langle j \rangle = e\mathcal{C}_{-}/T$ for $|\omega| > 4g$, it is dissipative and no longer quantized due to the band touching, in analogy with the photovoltaic Hall effect [24] in graphene. The photocurrent approaches the finite asymptotic value $\langle j \rangle = e\text{sign}(\omega)/\pi$ for $|\omega| \gg g$, which can be regarded as the lowest order, linear response correction to the current in g , hence the weak-coupling regime (Fig. 2).

Proposal for a measurement setup.- In practise, the weak coupling regime $g \ll |\omega|$ is usually realized. There a typical radiation field (magnetic field strength of the order of $10^{-4} - 10^{-5}$ T) yields a photocurrent of the order of 0.1 – 10 pA, depending on the effective g -factor values, which can be significantly enhanced ($g_{\text{eff}} \approx$

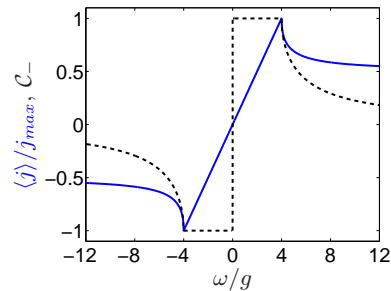


FIG. 2. (Color online) The induced photocurrent (blue solid line) and the \mathcal{C}_{-} Chern number (black dashed line) are shown as a function of the frequency ω . The photocurrent roughly behaves as $\langle j \rangle \approx e \text{sign}(\omega) \min(g, |\omega|/2)/\pi$ and it is maximal at the transition $|\omega| = 4g$ between the low and the high frequency regimes. The Chern number becomes non-quantized when band touching occurs at $4g = |\omega|$.

20 – 50) for materials with strong spin-orbit coupling like HgTe/CdTe, InAs/GaSb, HgSe or Bi₂Se₃. Such induced current can be detected in a contactless measurement. When the total area of the QSH insulator is exposed to the radiation field (i.e. the laser's spotsize is bigger than the area of the sample), a circulating loop current flows around the sample as in Fig. 1. A perpendicular magnetic field is induced according to the Biot-Savart law as $B_{\text{ind}} = \mu_0 2\sqrt{2} \langle j \rangle / \pi L$ with L the linear size of a square shaped sample (μ_0 the vacuum permeability), staying roughly constant within the sample. For $\langle j \rangle = 1$ pA and $L = 1$ micron, this gives $B_{\text{ind}} = 1$ pT. This induced magnetic field is within the detectability limit of an ac SQUID [23]. Finally standard 2 contacts measurement can also be used in order to detect the photocurrent. For a strip sample with laser's spot size bigger than the width but smaller than the length, backscattering is induced[29], which suppresses the photocurrent.

So far we have considered the idealistic situation for the generation of the dc-photocurrent, namely zero chemical potential in the QSH edge modes, strictly vanishing orbital effect and no inversion symmetry breaking. In the following we discuss how additional effects may influence the dc photocurrent (see also [23]).

Orbital effect and ac current response.- When the vector potential is taken into account (in the typical $v_F e A_0 / \omega \ll 1$ regime), an ac current develops on top of the dc one as $\langle j \rangle \approx j_{\text{dc}} + j_{\text{ac}} \cos(\omega t)$. We have solved Eq. (1) numerically [23] with the vector potential, and the results are shown in Fig. 3. The induced ac component stays always small compared to the dc one because the vector potential without the Zeeman term cannot cause spin-flip processes and is unable to generate any current. Indeed, the matrix element for optical transitions due to the vector potential is $\Phi_{+}(p, t)\sigma^z\Phi_{-}(p, t) = g/\lambda$. Therefore, the extended Kubo formula[27] predicts the scaling of the ac component as $j_{\text{ac}} \sim v_F e A_0$ [23].

Effect of the finite doping on the edge. So far we have

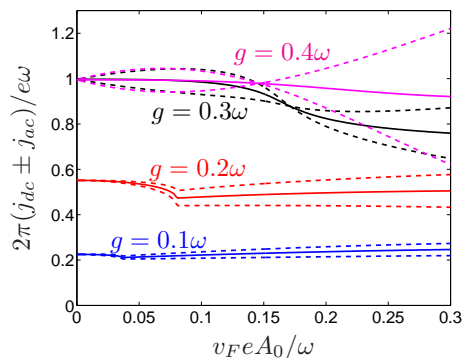


FIG. 3. (Color online) The induced dc (by the Zeeman term, solid line) \pm the ac (by the vector potential, dashed lines) currents are plotted as a function of the vector potential, for several values of g , j_{ac} is always smaller than j_{dc} for physically relevant parameters. The current behaves as $\langle j \rangle \approx j_{dc} + j_{ac} \cos(\omega t)$.

considered the optimal situation for photocurrent generation, namely zero Fermi energy in the QSH state. In the case of a finite chemical potential, the dc photocurrent vanishes gradually as we move away from half filling of the QSH edge states. The one-dimensional momentum acts as a polarizing effective magnetic field in Eq. (1). For large momenta $|p| \gg (|\omega|, |g|)/v_F$, this polarization is so strong that the circularly polarized magnetic field hardly induces any magnetization, while close to the Dirac point ($p \sim 0$), the magnetic field represented by the momentum is very weak, and the circularly polarized field dominates over the momentum. The induced, helicity dependent magnetization originates from these states living close to $p = \omega/2v_F$, as indicated by the non-trivial Aharonov-Anandan phase in this region [23].

Inversion symmetry breaking and static magnetic field.

We also consider the effect of a perturbation $g_0\sigma_x$ in the Hamiltonian Eq. (1) in order to mimic an eventual inversion symmetry breaking[22] and subsequent S^z non-conservation (as in HgTe/CdTe quantum wells). This static Zeeman term opens a gap at $p = 0$ whereas the dc-current is mainly built up from states near $p = \omega/2v_F$. Therefore the effect of inversion symmetry breaking on the dc-photocurrent is expected to be weak. Indeed we have checked that the dc current, and also the ac component (in presence of orbital effect), are almost identical to those of Fig. 3 for $g_0 < g$ [23].

Zitterbewegung. The trembling motion of the center of mass coordinate, is caused by interference between the positive and negative energy states (i.e. interband transitions)[36]. The topological invariant measures it indirectly through $\hat{\mathbf{d}}_{\alpha,p}(t)$ in Eq. (7). The position operator satisfies $\partial_t x = v_F \sigma^z =: v(t)$. Generalizing Ref. [36]

to non-equilibrium Floquet states, we find

$$\frac{v(t)}{v_F} = \left([\mathbf{n} \circ \mathbf{n} + (\mathbb{1} - \mathbf{n} \circ \mathbf{n}) \cos(2\lambda\tilde{t}) + \sin(2\lambda\tilde{t})\mathbf{n} \times] \boldsymbol{\sigma}_0 \right)_z \quad (12)$$

with $\mathbf{n} = \hat{\mathbf{d}}_{\alpha,p}(t_0)$, $\tilde{t} = t - t_0$, $\mathbf{n} \circ \mathbf{n}$ is the dyadic product and $\boldsymbol{\sigma}_0$ is the spin configuration at $t = t_0$.

Conclusion.- Radiation of a helical edge drives a transition between nondissipative charge pumping at low frequency and a high frequency dissipative regime, reflected in the behaviour of the photocurrent. Note that for (neutral) atoms in optical traps, one can introduce a Zeeman term without any orbital counterpart, or fabricate chiral edge states with spin quantized parallel to the momentum [11]: without any vector potential, the full transition from dissipationless to dissipative charge pumping can then be followed.

We acknowledge support by the Hungarian Scientific Research Fund No. K72613, K73361, K101244, CNK80991, the New Széchenyi Plan Nr. TÁMOP-4.2.1/B-09/1/KMR-2010-0002, by the European Research Council Grant Nr. ERC-259374-Sylo and by the Bolyai program of the Hungarian Academy of Sciences. JC acknowledges support from EU/FP7 under contract TEMSSOC and from ANR through project 2010-BLANC-041902 (ISOTOP).

* dora@kapica.phy.bme.hu

- [1] M. Z. Hasan and C. L. Kane, Rev. Mod. Phys. **82**, 3045 (2010).
- [2] X.-L. Qi and S.-C. Zhang, Rev. Mod. Phys. **83**, 1057 (2011).
- [3] C. L. Kane and E. J. Mele, Phys. Rev. Lett. **95**, 226801 (2005).
- [4] B. A. Bernevig, T. L. Hughes, and S.-C. Zhang, Science **314**, 1757 (2006).
- [5] C. Liu, T. Hughes, X.-L. Qi, K. Wang, and S.-C. Zhang, Phys. Rev. Lett. **100**, 236601 (2008).
- [6] C. Weeks and M. Franz, Phys. Rev. B **82**, 085310 (2010).
- [7] H.-M. Guo and M. Franz, Phys. Rev. B **80**, 113102 (2009).
- [8] K. Sun, H. Yao, E. Fradkin, and S. A. Kivelson, Phys. Rev. Lett. **103**, 046811 (2009).
- [9] L. Jiang, T. Kitagawa, J. Alicea, A. R. Akhmerov, D. Pekker, G. Refael, J. I. Cirac, E. Demler, M. D. Lukin, and P. Zoller, Phys. Rev. Lett. **106**, 220402 (2011).
- [10] T. D. Stanescu, V. Galitski, J. Y. Vaishnav, C. W. Clark, and S. Das Sarma, Phys. Rev. A **79**, 053639 (2009).
- [11] N. Goldman, I. Satija, P. Nikolic, A. Bermudez, M. A. Martin-Delgado, M. Lewenstein, and I. B. Spielman, Phys. Rev. Lett. **105**, 255302 (2010).
- [12] M. König, S. Wiedmann, C. Brune, A. Roth, H. Buhmann, L. W. Molenkamp, X.-L. Qi, and S.-C. Zhang, Science **318**, 766 (2007).
- [13] A. Roth, C. Bruene, H. Buhmann, L. Molenkamp, J. Maciejko, X.-L. Qi, and S.-C. Zhang, Science **325**, 294 (2009).

- [14] I. Knez, R.-R. Du, and G. Sullivan, *Phys. Rev. Lett.* **107**, 136603 (2011).
- [15] T. Kitagawa, E. Berg, M. Rudner, and E. Demler, *Phys. Rev. B* **82**, 235114 (2010).
- [16] A. P. Schnyder, S. Ryu, A. Furusaki, and A. W. W. Ludwig, *Phys. Rev. B* **78**, 195125 (2008).
- [17] X.-L. Qi, T. L. Hughes, and S.-C. Zhang, *Phys. Rev. B* **78**, 195424 (2008).
- [18] A. Kitaev, *AIP Conf. Proc.* **1134**, 22 (2009).
- [19] N. H. Lindner, G. Refael, and V. Galitski, *Nat. Phys.* **7**, 490 (2011).
- [20] J. Karch, P. Olbrich, M. Schmalzbauer, C. Zoth, C. Brinsteiner, M. Fehrenbacher, U. Wurstbauer, M. M. Glazov, S. A. Tarasenko, E. L. Ivchenko, D. Weiss, J. Eroms, *et al.*, *Phys. Rev. Lett.* **105**, 227402 (2010).
- [21] B. Wittmann, S. N. Danilov, V. Bel'kov, S. A. Tarasenko, E. G. Novik, H. Buhmann, C. Brüne, L. W. Molenkamp, Z. D. Kvon, N. N. Mikhailov, S. A. Dvoretzky, N. Q. Vinh, *et al.*, *Semicond. Sci. Technol.* **25**, 095005 (2010).
- [22] X.-L. Qi, T. L. Hughes, and S.-C. Zhang, *Nat. Phys.* **4**, 273 (2008).
- [23] see Supplementary material for further details.
- [24] T. Oka and H. Aoki, *Phys. Rev. B* **79**, 081406 (2009).
- [25] D. S. L. Abergel and T. Chakraborty, *Nanotechnology* **22**, 015203 (2011).
- [26] J.-i. Inoue and A. Tanaka, *Phys. Rev. Lett.* **105**, 017401 (2010).
- [27] Y. Zhou and M. W. Wu, *Phys. Rev. B* **83**, 245436 (2011).
- [28] P. Hosur, *Phys. Rev. B* **83**, 035309 (2011).
- [29] M. J. Schmidt, E. G. Novik, M. Kindermann, and B. Trauzettel, *Phys. Rev. B* **79**, 241306 (2009).
- [30] H. Calvo, H. Pastawski, S. Roche, and L. Torres, *Appl. Phys. Lett.* **98**, 232103 (2011).
- [31] T. Kitagawa, T. Oka, A. Brataas, L. Fu, and E. Demler, arXiv:1104.4636.
- [32] H. Sambe, *Phys. Rev. A* **7**, 2203 (1973).
- [33] T. Dittrich, P. Hanggi, G.-L. Ingold, B. Kramer, G. Schon, and W. Zwerger, eds., *Quantum Transport and Dissipation* (Wiley-WCH, Weinheim, 1998).
- [34] A. M. J. Schakel and G. W. Semenoff, *Phys. Rev. Lett.* **66**, 2653 (1991).
- [35] D. J. Thouless, *Phys. Rev. B* **27**, 6083 (1983).
- [36] J. Cserti and Gy. Dávid, *Phys. Rev. B* **74**, 172305 (2006).
- [37] J. H. Shirley, *Phys. Rev.* **138**, B979 (1965).
- [38] J. Goldstone and F. Wilczek, *Phys. Rev. Lett.* **47**, 986 (1981).
- [39] Y. Aharonov and J. Anandan, *Phys. Rev. Lett.* **58**, 1593 (1987).
- [40] L. Barron, *Molecular Light Scattering and Optical Activity* (Cambridge University Press, Cambridge, 2004).

**SUPPLEMENTARY ONLINE MATERIAL FOR
"OPTICALLY ENGINEERING THE
TOPOLOGICAL PROPERTIES OF A SPIN HALL
INSULATOR"**

**DERIVATION OF THE ELECTRIC CURRENT
OPERATOR**

The electric current operator can be obtained from the continuity equation, which, in one dimension, reads as

$$\frac{\partial \rho(x)}{\partial t} + \frac{\partial j_x}{\partial x} = 0. \quad (13)$$

In our case, the charge density operator is $\rho(x) = e(c_\uparrow^\dagger(x)c_\uparrow(x) + c_\downarrow^\dagger(x)c_\downarrow(x))$, where $c_\sigma(x)$ annihilates a particle with spin σ at position x . The time derivative can be evaluated from

$$\begin{aligned} \frac{\partial \rho(x)}{\partial t} &= i[H, \rho(x)] = -ev \frac{\partial}{\partial x} (c_\uparrow^\dagger(x)c_\uparrow(x) - c_\downarrow^\dagger(x)c_\downarrow(x)) = \\ &= -\frac{\partial j_x}{\partial x}. \end{aligned} \quad (14)$$

From this, the current operator is obtained in second quantized form as $j_x = ev(c_\uparrow^\dagger c_\uparrow - c_\downarrow^\dagger c_\downarrow)$, or in first quantized form as $j_x = ev\sigma^z$.

**INFLUENCE OF THE VECTOR POTENTIAL
AND OTHER TERMS**

Vector potential

The effect of the vector potential can be investigated more rigorously, after performing a unitary transformation as $\Psi_p(t) = U_p(t)\tilde{\Psi}_p(t)$ with $U_p(t) = \exp(i\sigma^z v_F e A_0 \sin(\omega t)/\omega)$. As a result, the Hamiltonian changes (together with the $-iU_p^\dagger(t)\partial_t U_p(t)$ term, coming from the time-dependent unitary transformation) to

$$H = v_F \sigma^z p + g \left[\sigma^+ \exp(-i\omega t - i2v_F e A_0 \sin(\omega t)/\omega) + \sigma^- \exp(i\omega t + i2v_F e A_0 \sin(\omega t)/\omega) \right]. \quad (15)$$

The exponential term in the off-diagonal can be simplified using the Jacobi-Anger expansion as

$$\exp(i2z \sin(\omega t)) = \sum_{m=-\infty}^{\infty} J_m(2z) \exp(im\omega t), \quad (16)$$

$z = v_F e A_0/\omega$, $J_m(2z)$ is the m th Bessel function of the first kind. Higher harmonics in ωt appear in σ^+ and also σ^- , triggering transitions between the eigenstates of σ^z . This can be simplified in the limit of $|z| \ll 1$ using the expansion of the Bessel functions ($J_m(2z) \rightarrow (\text{sign}(m)z)^{|m|}/|m|!$ for small z), which translates to $v_F e E_0 \ll \hbar\omega^2$ (upon reinserting original units). In this case, only the $m = 0$ component needs to be

taken into account, the higher harmonics can safely be neglected or treated perturbatively.

In terms of the higher harmonics of the vector potential, we can take them potential perturbatively into account. The higher harmonics in ωt from Eq. (16), appearing after the unitary transformation, would dynamically open small gaps in the DOS, in addition to the main dynamical gaps from one-photon processes around $\pm\omega/2$ with size g , at integer multiples of $\omega/2$. Their size is estimated in the $g \ll \omega$ limit as

$$\Delta_m \sim \frac{g}{|m|!} \left(\frac{v_F e E_0}{\omega^2} \right)^{|m|} \ll g \text{ for } m \neq 0, \quad (17)$$

corresponding to multi-photon excitations, similarly to graphene radiated with circularly polarized light[24, 27]. While the Δ_0 dynamical gap is generated solely by the circularly polarized magnetic fields, higher gaps are triggered by the vector potential term, though these are negligible.

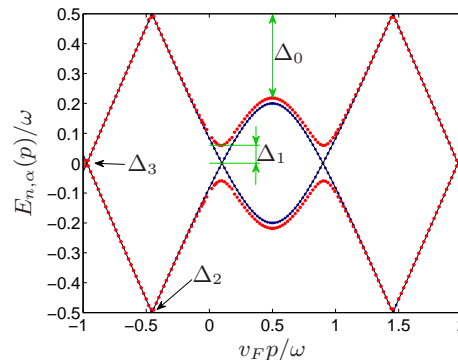


FIG. 4. (Color online) The Floquet quasienergies are shown in the Floquet Brillouin zone ($|E_{n,\alpha}(p)| < |\omega|/2$) for $g = 0.3\omega$. The black solid line/blue dots denote the analytical result from Eq. (3) in the main text/the numerical solution of Eq. (1) in the main text with $A_x = 0$, hardly distinguishable from each other. The red dots stem from the numerical solution of Eq. (1) in the main text with $z = v_F e E_0/\omega^2 = 0.2$, the dynamical gaps are denoted by the green vertical arrows, showing good agreement with the prediction of Eq. (17) as $\Delta_0 = 0.3\omega$, $\Delta_1 = 0.06\omega$, $\Delta_{2,3}$ are invisible on this scale. The vector potential is indeed negligible for $v_F e E_0 \ll \omega^2$, as conjectured using the Jacobi-Anger expansion, and only the circularly polarized magnetic field needs to be considered in this parameter range.

To check the opening of additional dynamical gaps, we have evaluated the Floquet quasienergies of the edge state by the physically transparent, yet unorthodox method of following the adiabatic time evolution of the initial eigenstates of Eq. (1) in the main text with $A_0 = g = 0$, namely $(0, 1)^T$ and $(1, 0)^T$. Both the vector potential and the Zeeman coupling are switched on at $t \rightarrow -\infty$ in an adiabatic manner, by attaching the $\exp(-\delta|t|)$ factor ($\delta \rightarrow 0^+$) to them, and letting them evolve till $t = 0$. The resulting quasiener-

gies within the Floquet Brillouin zone [32, 33] are determined from the numerically evaluated wavefunction as $E = \omega \ln[\Psi(t=0)/\Psi(t=T)]/2\pi i$, devised by Eq. (2) in the main text, shown in Fig. 4. As seen, the numerical procedure agrees convincingly with the analytic prediction of Eq. (3) in the main text. The main gap at $v_F p = \omega/2$ of size g from the Zeeman term dominates and the higher order dynamical gaps due to the vector potential are indeed negligible for $v_F e E_0/\omega^2 \ll 1$, in accordance with Eq. (17). Among the higher order dynamical gaps, Δ_1 opens a tiny gap around the Dirac point $E = 0$.

We have also solved our Floquet problem following the more conventional approach as in Ref. 37, by making use of the time periodicity of the Hamiltonian. There, by close analogy to Bloch states, the initially time dependent Schrödinger equation can be represented as a time independent matrix equation, whose various entries denote the matrix elements between Floquet states. Then, the resulting eigenvalue problem is solved by truncating this matrix to a given size, corresponding to the allowed maximal photon excitations or the number of considered Floquet quasienergies. The obtained Floquet eigenenergies and eigenfunctions are then used to calculate numerically the average energy to determine the proper filling, and then to evaluate the induced dc and ac component of the current. In general, the vector potential induces all higher harmonics of ω to the current as $\cos(n\omega t)$ with n integer. However, in the physically relevant case, when $v_F e A_0 \ll \omega$, the $\cos(\omega t)$ dominates over the other terms, and the resulting current reads as

$$\langle j \rangle \approx j_{dc} + j_{ac} \cos(\omega t). \quad (18)$$

This is plotted in Fig. 3 of the main text, allowing for 80 photons or equivalently 80 Floquet bands. We have also checked that the results do not depend on the number of considered Floquet bands in this range. Usually, $j_{ac} \ll j_{dc}$ in the $(g, v_F e A_0) \ll \omega$ regime, because the vector potential in itself cannot induce any current, only when the Zeeman term is included.

In the regime of adiabatic charge pumping $(\omega, v_F e A_0 \ll g)$, the Goldstone-Wilczek formula[22, 38] can be used to evaluate the current from Eq. (15) as

$$\langle j \rangle = \frac{e}{2\pi} (\omega + 2v_F e A_0 \cos(\omega t)), \quad (19)$$

corroborating our numerical findings. Note that a finite g is essential to induce any current, although its explicit value drops out from the above expression.

Inversion symmetry breaking

We also consider the effect of an additional term in the Hamiltonian, which is a static Zeeman term in the x

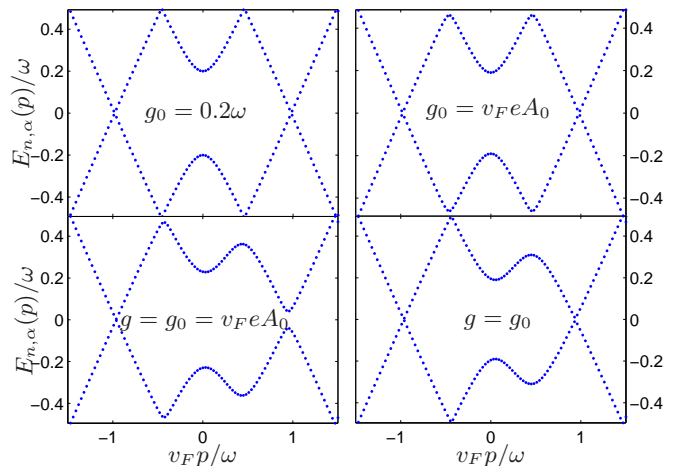


FIG. 5. (Color online) The Floquet quasienergies are shown in the Floquet Brillouin zone in the presence of a static perpendicular Zeeman field, mimicking inversion symmetry breaking. Top left: $g_0 = 0.2\omega$, $g = A_0 = 0$; top right: $g_0 = v_F e A_0 = 0.2\omega$, $g = 0$; bottom left: $g = g_0 = v_F e A_0 = 0.2\omega$; bottom right: $g = g_0 = 0.2\omega$. The main effect of the static Zeeman term is the opening of a gap $\sim g_0$ around $p = 0$.

direction as

$$H' = g_0 \sigma^x, \quad (20)$$

i.e. perpendicular to the spin quantization axis of the QSH edge state. A σ^y term would have identical effect. This can be thought of as mimicking inversion symmetry breaking[22], since the edge state gap induced by the perpendicular static magnetic field is non-zero. Usually, the static in-plane field g_0 is small and does not modify qualitatively the physics discussed so far. We have evaluated numerically the Floquet bandstructure due to this additional static field in the presence and absence of circularly polarized Zeeman and orbital terms. The main effect of g_0 is to open a gap around $p \sim 0$ of size g_0 , as can be checked in Fig. 5.

In terms of the induced current, when $g = 0$, the additional static term can only induce a tiny ac current without any dc component, whose magnitude is comparable to that shown in Fig. 3 in the main text. When $g_0 \ll g$, which is the physically relevant regime, the induced current is almost identical to that in Fig. 3 in the main text, including both a dc and ac components. Only when g_0 is comparable to g , the above picture is modified and even in the absence of a vector potential, both dc and ac currents are induced by the interplay of the static and circularly polarized Zeeman fields.

Two circularly polarized electromagnetic fields

The case with two circularly polarized electromagnetic fields with different frequencies (ω_1 and ω_2) can be con-

sidered via the Hamiltonian

$$H(t) = v_F \sigma^z p + [\sigma^+ (g_1 e^{-i\omega_1 t} + g_2 e^{-i\omega_2 t}) + h.c.], \quad (21)$$

neglecting the vector potential for simplicity. In the topologically protected region ($\omega_{1,2} \ll g_{1,2}$), when the periods are commensurate to each other with lowest common multiple $T = c_1 T_1 = c_2 T_2$ ($c_{1,2}$ integers), adiabatic charge pumping occurs. The dc photocurrent, which is the quantized charge adiabatically pumped through the system per cycle T , is calculated from the Goldstone-Wilczek formula[22, 38] as

$$\langle j \rangle = \frac{e}{4\pi} ((\omega_1 - \omega_2) \text{sign}(g_1^2 - g_2^2) + \omega_1 + \omega_2), \quad (22)$$

giving $\langle j \rangle = e\omega_1/2\pi = ec_1/T$ for $g_1 > g_2$ and $\langle j \rangle = e\omega_2/2\pi = ec_2/T$ for $g_2 > g_1$. For incommensurate frequencies, continuity suggests that this relation still holds[35]. In addition, the two frequencies also induce an ac current with lowest harmonics as

$$j_{ac}(t) = -\frac{eg_1 g_2 (g_1^2 - g_2^2) (\omega_1 - \omega_2)}{2\pi (g_1^2 + g_2^2)^2} \cos[(\omega_1 - \omega_2)t]. \quad (23)$$

For large frequencies (and small couplings), we can use linear response theory to obtain the average dc current as $\langle j \rangle = e [g_1 \text{sign}(\omega_1) + g_2 \text{sign}(\omega_2)] / \pi$.

This also explains quantitatively what happens to the Floquet edge state in a static magnetic field. By setting $\omega_2 = 0$, g_2 represents a static Zeeman term in the x direction as $g_2 \sigma^x$. From Eq. (22), the dc current remains unchanged for $g_2 < g_1$ with respect to its zero static field value as $\langle j \rangle = e\omega_1/2\pi$, and drops to zero for $g_2 > g_1$, i.e. the static field destroys the adiabatic charge pumping when it becomes comparable to the circularly polarized component.

In summary, the typical hierarchy of energy scales in a condensed matter realization of the QSH edge state is $g_0 < g < v_F q A_0 < \omega$. In this case, as we have demonstrated, the induced dc current is mainly determined by the circularly polarized Zeeman term, while an additional, smaller ac component $\sim \cos(\omega t)$ arises from the orbital effect. In cold atoms, the Zeeman term can be realized without the orbital counterpart, thus only a purely dc current is induced.

DENSITY OF STATES

The density of states (DOS, $\rho(E)$) is evaluated from the overlap of two wavefunctions, one in which a particle is created in a given state in the initial wavefunction and then it is evolved in time until t , and the other, where the initial wavefunction is evolved in time and then an

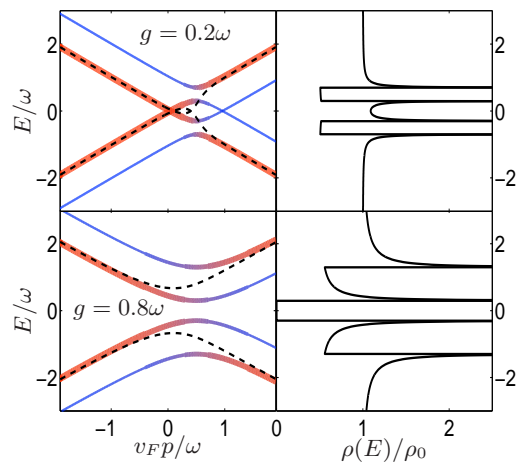


FIG. 6. (Color online) The quasienergies (left panel) and the corresponding density of states (right panel) are shown for $g/\omega = 0.2$ (upper) and 0.8 (lower). The spectral weight in the spectrum increases from the blue and thin lines to red and thick ones. The black dashed line denotes the average energy from Eq. (5) in the main text. For $g = 0$, the DOS is constant. In the static case, a gap opens around zero energy. With increasing ω , the gaps are shifted to $\pm\omega/2$, carrying only half of the spectral weight. For $g > \omega/2$, a clean gap remains around zero energy, but new gap edges show up at $\pm\omega/2 \pm g$. For larger frequencies, the gap disappears, and a plateau develops around zero energy in the DOS at $\rho_0/2$.

extra particle is added at t . The temporal Fourier transform of the time dependent overlap yields

$$\begin{aligned} g_p(E) &= i \int_0^\infty dt \exp[iEt - t\delta] \Psi_p^+(t) \Psi_p(0) = \\ &= i \int_0^\infty \frac{dt}{2\lambda} \exp[i(E + E_\alpha(t))t - t\delta] \times \\ &\times [\lambda + \alpha(v_F p - \omega/2) + \exp(-i\omega t)(\lambda - \alpha(v_F p - \omega/2))], \end{aligned} \quad (24)$$

where $\delta \rightarrow 0^+$. This gives (see Fig. 2 in the main text)

$$\rho(E) = \frac{1}{\pi} \sum_{p,\alpha} \text{Im} g_p(E) = \frac{\rho_0}{2} \sum_{s=\pm 1} \frac{|E + s\omega/2|}{\sqrt{(E + s\omega/2)^2 - g^2}} \quad (25)$$

with $\rho_0 = a/\pi v_F$, a the lattice constant. Following the steps outlined in Refs. 24, 25, and 27, one obtains the very same expression for the DOS, shown in Fig. 6 together with the Floquet and average energies. In addition to $E_\alpha(p)$, another branch with quasienergy $E_\alpha(p) - \omega$ appears due to the spinor structure of the wavefunction. The spectrum with positive or negative velocity ($\partial_p E_\alpha(p) > 0$ or $\partial_p E_\alpha(p) < 0$) hosts dominantly up or down spin electrons, respectively. Due to the circular magnetic field, these components are mixed and for small

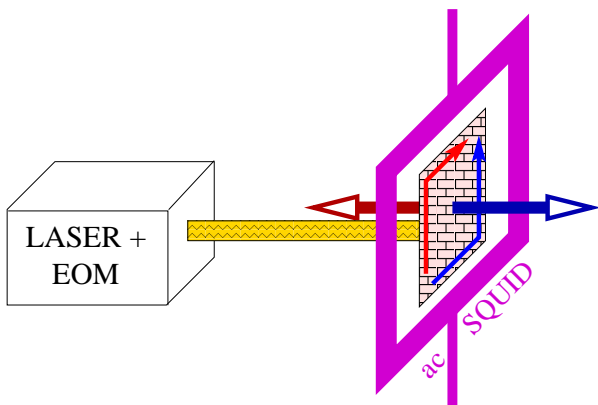


FIG. 7. (Color online) The proposed experimental scheme for the detection of the photoinduced current. A linearly polarized radiation field is transformed to circularly polarized one by an electro-optical modulator (EOM)[40], and the helicity of the polarization is changed periodically in time, with a frequency in the few 100 Hz range. The sample is denoted by the brick wall lattice filled plane. The direction of the photocurrent (red and blue arrows within the plane of the sample) as well as the induced magnetic field (red and blue arrows perpendicular to the plane of the sample) depend on the helicity of the polarization, B_{ind} is measured with an ac SQUID.

m , the up/down spin branch develops a weak down/up spin character, respectively.

AHARONOV-ANANDAN PHASE

Through the time dependent Zeeman effect, the spin evolves cyclically with period T , and the wavefunction picks up the Aharonov-Anandan [39] phase:

$$\gamma = \int_0^T dt \Phi_\alpha^+(p, t) i \partial_t \Phi_\alpha(p, t) = \pi \left(\frac{\alpha(v_F p - \omega/2)}{\lambda} - 1 \right). \quad (26)$$

For large momenta, this dynamical phase hardly changes with the parameters g and ω , and is pinned to the trivial value $\gamma \simeq -2\pi\Theta(-\alpha p)$. By contrast, for $p = \omega/2$, it takes the non-trivial value $-\pi$, signaling that states close to $p = \omega/2v_F$ are the most influenced by the radiation field.

POSSIBLE EXPERIMENTS

Technically, a linearly polarized light can be run through an electro-optical modulator (EOM), producing

circularly polarized light[40], as shown in Fig. 7. This can also change the helicity of the polarization periodically in time, with a frequency in the few 100 Hz range (i.e. much smaller than that of the radiation field), resulting in a sign change of the induced magnetization, B_{ind} (pointing upwards vs. downwards with respect to the plane of the QSH insulator), facilitating the experimental observation. The induced magnetization stemming from the loop current can be detected by an ac SQUID (purple frame around the sample). By using the Biot-Savart law, the magnetic field profile along a cut through a square shaped sample is shown in Fig. 8, which divides it into two identical rectangles. Qualitatively similar fields are induced along other directions. The divergence at the edges is cut-off by the finite spatial extension of the edge states.

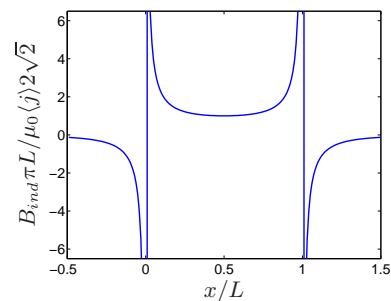


FIG. 8. (Color online) The induced magnetic field is shown, calculated from the Biot-Savart law, staying rather flat within the sample ($0 < x < L$).

The induced current can also be detected directly using more conventional techniques. By irradiating only one edge of the sample and adding contacts to its ends, one could in principle measure the induced photocurrent, as shown in Fig. 9

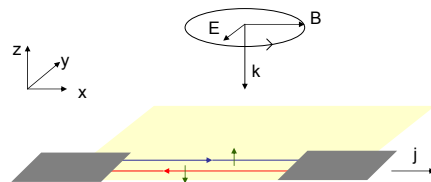


FIG. 9. (Color online) Radiated single edge with contacts, designed the measure the photoinduced current directly.